Crystallinity Development in Cellular Poly(lactic acid) in the Presence of Supercritical Carbon Dioxide

Mihaela Mihai,[1,2] Michel A. Huneault,[1] Basil D. Favis[2]

[1]*National Research Council of Canada, Industrial Materials Institute, 75 de Mortagne, Boucherville, Québec, Canada J4B 6Y4*
[2]*CREPEC, Chemical Engineering Department, École Polytechnique de Montréal, P.O. Box 6079, Station Centre-Ville, Montréal, Québec, Canada H3C 3A7*

Received 21 August 2008; accepted 25 February 2009
DOI 10.1002/app.30338
Published online 1 May 2009 in Wiley InterScience (www.interscience.wiley.com).

ABSTRACT: This article investigates the crystallinity development in cellular poly(lactic acid) (PLA) and the effect of the achieved crystalline content on its properties and microstructure. Carbon dioxide (CO_2) in its supercritical state was used as the expansion agent for three different grades of PLA that differed in terms of *L*-lactic acid content. Cellular PLA was produced on a twin-screw extrusion line using capillary dies of various diameters. The obtained crystalline contents were measured by differential scanning calorimetry and X-ray diffraction techniques. The morphology of the cellular structures was examined using scanning electron microscopy. The crystallinity developed on expansion depended on *L*-lactic acid content, on supercritical CO_2 concentration, polymer flow rate, and die diameter. Cellular PLA, with densities as low as 30 kg/m^3, was obtained under the most favorable conditions. It was shown that the crystallinity development in PLA enhances its cellular structure formation and enables the fabrication of quality cellular materials at lower CO_2 concentration. The presence of PLA crystallites within expanded cell walls leads to a peculiar 2D-cavitation phenomena observed only in the cell walls of semicrystalline foams. © 2009 Wiley Periodicals, Inc. J Appl Polym Sci 113: 2920–2932, 2009

Key words: poly(lactic acid); crystallization; carbon dioxide; foam extrusion

INTRODUCTION

Poly(lactic acid) (PLA) is a rigid and transparent bio-based polymer obtained from the ring-opening polymerization of lactide, a lactic acid dimer.[1] Lactic acid (LA) has two optically active configurations known as *D*-LA and *L*-LA. The *L* form is the most common in nature and therefore is the main constituent of commercially available PLA. Minor amounts of *D*-LA are typically used to control the crystallinity of PLA since the *D*-LA units will disrupt the crystallization of the *L*-LA chains. PLA obtained from a feedstock comprising more than 15% of *D*-LA will be completely amorphous. The crystalline level increases with monomer purity to reach around 45% for the pure poly(*L*-lactide). The melting temperature also increases with purity from 140°C for a 15/85 *D*/*L* ratio to 178°C for pure poly(*L*-lactide).[2] The level of crystallinity affects the mechanical properties, the permeability, the heat deflection temperature, and the time of degradation in a composting environment.[3]

PLAs properties are often compared with those of polystyrene (PS) and polyethylene terephthalate (PET). One important difference is its glass transition temperature, around 57°C, significantly lower than that of PS and PET.[4,5] This will limit the PLA utilization unless it can be properly crystallized during processing. Unfortunately, its rate of crystallization is relatively low because of its high chain rigidity. Crystallization of PLA in isothermal or nonisothermal conditions has been investigated by many authors.[6–11] Significant crystallinity has been achieved in PLA through the use of different nucleation agents that increases the heterogeneous nucleation density[12–17] or of plasticizers that widens the crystallization window by increasing the PLA chain mobility and decreasing the glass transition temperature.[18–23] Simultaneous use of nucleant and plasticizers were also reported to have a synergistic effect enabling significant crystallization within an injection molding cycle.[24]

The use of CO_2 as a physical blowing agent in polymer materials also has a significant plasticization effect that in turn could affect the crystallization rate.[25] Strain-induced nucleation is another factor that could contribute to crystallinity development in PLA. A development of crystalline structure was observed for PLA films during uniaxial and biaxial

Correspondence to: M. A. Huneault (michel.huneault@cnrc-nrc.gc.ca).

Contract grant sponsor: Canada's Natural Science and Engineering Research Council, Canadian Biomass Innovation Network.

stretching.[26,27] In the stretching processes, high crystallinity levels can be achieved within a relatively short time and at much lower temperature than under quiescent crystallization conditions. Similarly, the rapid foam expansion involves biaxial deformation of foam cell walls that could initiate faster crystallization than in other processes that do not involve high levels of orientation. Nevertheless, little work has been published on the extrusion foaming of PLA.[28,29]

The objective of the current work is to investigate the relation between crystallization and CO_2 foaming of semicrystalline PLA. For this purpose, PLA with different *D*-LA content are to be foamed using various CO_2 concentrations, melt flow rates, and die diameters to observe the effect on crystallinity development in relation to foam properties. Independent experiments on the effect of biaxial stretching and of CO_2 concentration on crystallinity development will be carried out in an attempt to separate the effect of these various factors and to draw general conclusions on the relations between the crystallinity development and foaming of PLA.

EXPERIMENTAL

Materials

Three PLA grades supplied by NatureWorks were selected. PLA1 and PLA2 were semicrystalline grades, PLA 4032D and PLA 2002D, respectively, with approximately 2% and 4% of *D*-lactic acid monomer. PLA3 was a completely amorphous grade, PLA 8302D, in which, according to the supplier, the *D*-lactic acid content was 10%. All PLA were dried at 65°C for a minimum of 8 hr before use. CO_2 with a purity of 99.9% was used as blowing agent in the PLA foam extrusion process.

Extrusion foaming process

The extruder used in the foaming process was a Leistritz 34 mm corotating twin-screw extruder comprising 12 barrel zones numbered from 0 to 11. The process configuration is presented in Figure 1. The CO_2 was pumped into barrel segment 7 using a high-pressure pump. The rest of the extruder was used to solubilize the blowing agent in the polymer melt and to bring the material temperature to the desired final extrusion temperature. The screw configuration was especially designed to conceal the high CO_2 pressure in the latter portion of the extruder. This was achieved by placing a pair of reverse screw elements upstream from the blowing agent injection point. These screw elements generated a restriction to polymer flow, increased the pressure locally, and thus created a polymer melt seal that prevented leakage of the blowing agent upstream. A gear pump was also placed at the end of the extrusion line to maintain a high-pressure level in the extruder. The extruder was operated at a constant screw rotation speed of 150 rpm. Three different capillary dies were used with diameters of 1.5, 2, and 3.5 mm. These different dies were used with the purpose of varying the die pressure drop and to asses its effect on the achieved foam crystallinity. All foam samples were stored for 2 weeks at room temperature before crystallinity measurement to make sure that the CO_2 had diffused out of the samples. The samples were dimensionally stable during that period.

Biaxial stretching

To investigate the effect of biaxial stretching on PLA crystallinity, PLA1 and PLA2 were extruded into sheets, biaxially stretched, and tested for crystallinity content using differential scanning calorimetry (DSC) and X-ray diffraction (XRD). The nonoriented 0.5-mm thick sheets were produced on a RandCastle 12-mm cast film line. Square samples, 100 × 100 mm^2, were cut out of the central part of the 200-mm wide extruded sheets. These were biaxially stretched at 100°C using a Brückner Biaxial Lab Stretcher at a constant stretch speed of 1 m/min in both machine and transverse directions. Stretch ratios up to 9 × 9 were attained. A temperature equilibration time of 60 s was used in all cases to bring the sample temperature to the stretching temperature. It was

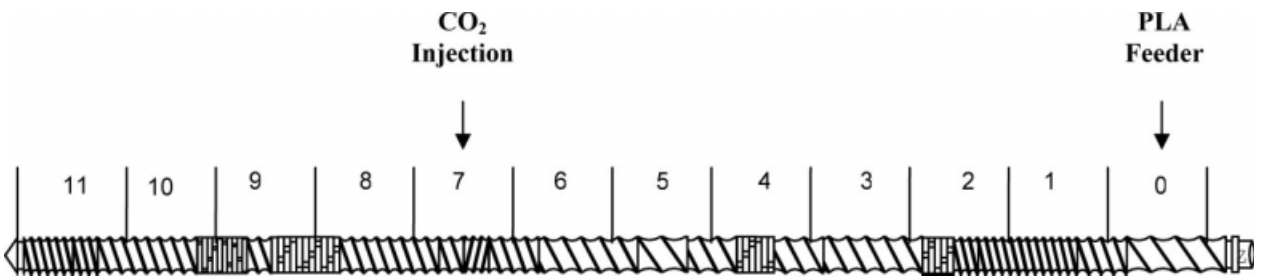

Figure 1 Twin-screw configuration used to foam the PLA.

verified that this equilibration time did not induce significant crystallization in PLA.

Crystallization under CO_2 pressure

PLA1 and PLA2 cast sheet samples were exposed to CO_2 at a pressure of 6 MPa and at ambient temperature using an autoclave. The exposure time was varied between 1 min and 2 h. Because of the time required to increase and decrease CO_2 pressure in the autoclave, exposure times shorter than 1 min were not achievable. After exposure, the sheets were allowed to equilibrate at ambient temperature for 24 h and then were tested for crystallinity content using DSC and XRD.

Differential scanning calorimetry

DSC analysis was carried out on a Perkin-Elmer Pyris 1 apparatus. The DSC was calibrated using an indium standard. For the initial crystallization measurements, the samples were heated from 20 to 200°C at 20°C/min, and the enthalpy of crystallization on heating ΔH_c and melting enthalpy ΔH_m were measured. The initial crystalline content in the samples was given by $(\Delta H_m - \Delta H_c)/\Delta H_f$ where ΔH_f is the theoretical heat of fusion of 100% crystalline PLA. A value of 93 J/g was taken for PLAs theoretical heat of fusion.[30] After the initial crystallinity measurements, the samples were maintained at 200°C for 5 min to erase the thermal history, cooled to 20°C at 20°C/min and then reheated again to 200°C at 20°C/min. In addition, isothermal crystallization from the amorphous state was used to measure the crystallization rates of the three pure PLA. In this case, the samples were heated, maintained at 200°C for 5 min and then cooled at −100°C/min down to 20°C to quench the samples in an amorphous state. They were rapidly reheated to the isothermal crystallization temperature, 100°C, and maintained at that temperature for 5 h to obtain a complete crystallization of the samples. The samples were finally reheated from 100 to 200°C at a rate of 20°C/min to measure the melting endotherm.

X-ray diffraction

XRD intensity of the foamed products, stretched sheets, and CO_2 saturated sheets were obtained with an X-ray diffractometer (D-8, Bruker). The samples were exposed to an X-ray beam with the X-ray generators running at 40 kV and 40 mA. The scanning was carried out at a rate of 0.03°/s in the angular region (2θ) of 2–40°. The foams were compressed at room temperature using a Carver Press for 5 min to collapse the foam structure and to make dense bars. Then, the surface of the bars was carefully smoothed using fine sand paper to remove any skin on the sample surface and to access the bulk of the material. The crystallinity fraction X_C in samples was quantified based on the ratio of the crystalline peak area I_C over the sum of $I_C + I_A$, where I_A is the area of the amorphous background for the same material.

Foam characterization

Scanning electron microscopy (SEM) was carried out on cryogenically fractured foam surfaces perpendicular to the extrusion direction. All foamed surfaces were sputter coated with a gold/palladium alloy or platinum before the observation. The density of the foams was determined by a water displacement method. At least three specimens were used for each formulation.

RESULTS

Extrusion foaming of the three selected PLA grades was carried out at CO_2 concentrations of 5, 7 and 9% CO_2. Extrusion with 3% CO_2 was also attempted but did not lead to much foaming and, therefore, this condition was discarded. We will examine first the DSC scans of these foams presented in Figure 2. It is noteworthy that, at the time of DSC testing, CO_2 was expected to have completely diffused out of the samples and thus the observed results were due to crystallization that occurred during the foaming process. The PLA1 foamed with 5% and 7% CO_2 crystallized on heating due to their uncompleted crystallizations during foaming. The 9% CO_2/PLA1 foam did not show any crystallization exotherm on heating, indicating that it had already been reached its maximum crystallinity level. The peak crystallization temperatures were 120 and 90°C for 5 and 7% CO_2 samples. Similar behavior was observed for PLA2 but with smaller crystallization levels and melting peaks in the first heating run. The peak crystallization temperature also decreased with the CO_2 concentration used during foaming. During the cooling cycle, no crystallization was observed for any sample. Even if the cooling rate was as low as 20°C/min, PLA1 or PLA2 could not crystallize under quiescent conditions. Therefore, in the second heating cycle, larger crystallization exotherms in the 110–150°C range were observed for foamed PLA1 followed by the corresponding melting endotherms. The peak areas decreased with the CO_2 concentration used in the foaming process possibly due to slight changes in chain scission or oligomer content. The samples obtained from PLA2 foams did not show any crystallization on the second heating. In the case of PLA3, DSC analysis confirmed its overall amorphous behavior, with no foam crystallinity and no crystallization on heating or cooling.

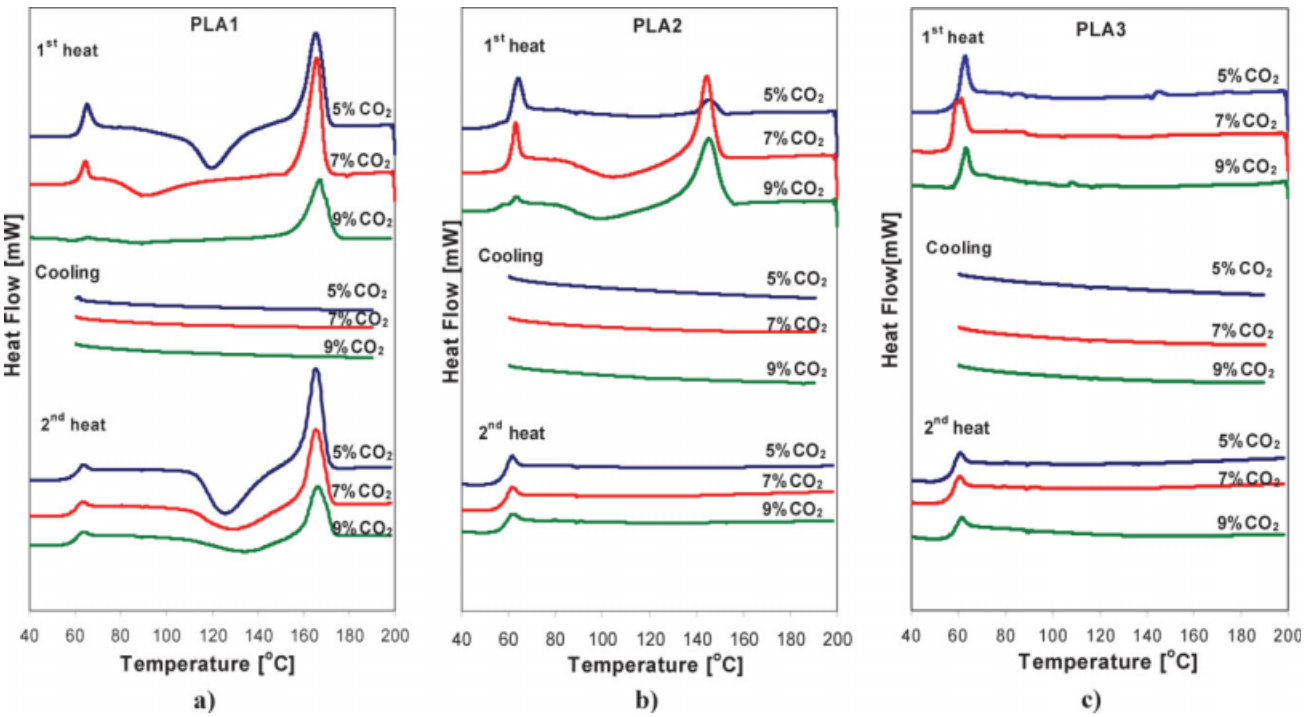

Figure 2 DSC traces for PLA foamed at a rate of 10 kg/h using 2-mm die. (a) PLA1, (b) PLA2, and (c) PLA3. [Color figure can be viewed in the online issue, which is available at www.interscience.wiley.com.]

The PLA foam crystallinity developed at different CO_2 concentrations are summarized in Figure 3 as a function of the nominal *D*-LA content. The crystallinity of PLA foams decreased from PLA1 to PLA3 as expected from the increasing *D*-LA content. In the case of PLA1, the foam crystallinity reached 45% when 9% CO_2 was used. For PLA2, the maximum crystallinity was 18% whereas for PLA3 no crystallinity was developed. It must be emphasized here that the pristine PLA1 and PLA2 do not readily crystallize under quiescent conditions. As we will discuss later (Fig. 7), the full crystallization in isothermal conditions was achieved within hours in contrast with a few seconds at the end of the extrusion foaming process.

Figure 4 presents SEM micrographs of fractured foam surfaces obtained for the three different PLA samples at 5, 7, and 9% CO_2. Foam density values are given under each micrograph. For 5% CO_2, the foam morphology was coarse and the foam densities ranged from 400 to 1000 kg/m^3 from PLA1 to PLA3, respectively. At 7% CO_2, the morphology was greatly improved for PLA1 and PLA2 and corresponded to fully expanded foams with thin cell walls and more or less hexagonal cell shapes. PLA1 had relatively uniform cells with dimensions in the 75–100 μm range. For PLA2, foam cells were slightly bigger, around 100–150 μm. Foam densities measured for these samples were around 30–40 kg/m^3. PLA3 showed a small decrease in cell dimensions compared with 5% CO_2 but still had a nonuniform cell dimension distribution, high thickness of cell walls and a high density of 300 kg/m^3. At 9% CO_2, all foams were fully expanded and low densities were obtained for all three PLA grades. It should be noted that for semicrystalline PLA1 and PLA2, it

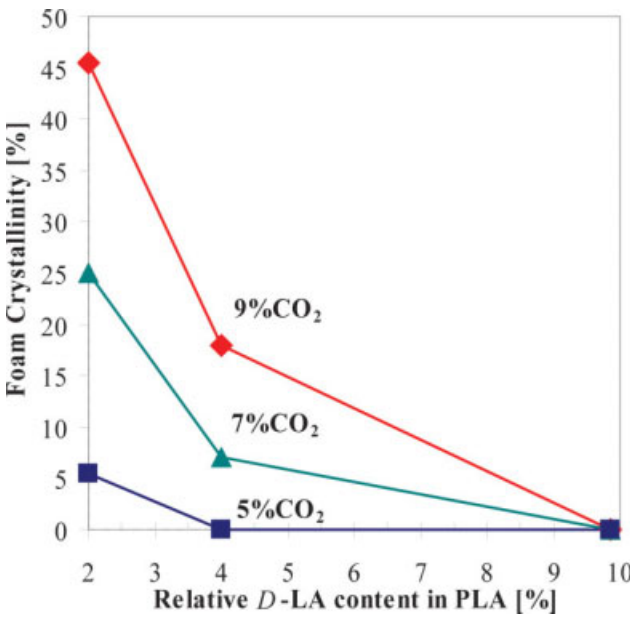

Figure 3 Foam crystallinity achieved at different CO_2 levels as a function of the nominal *D*-lactic acid content for the selected PLA grades. [Color figure can be viewed in the online issue, which is available at www.interscience.wiley.com.]

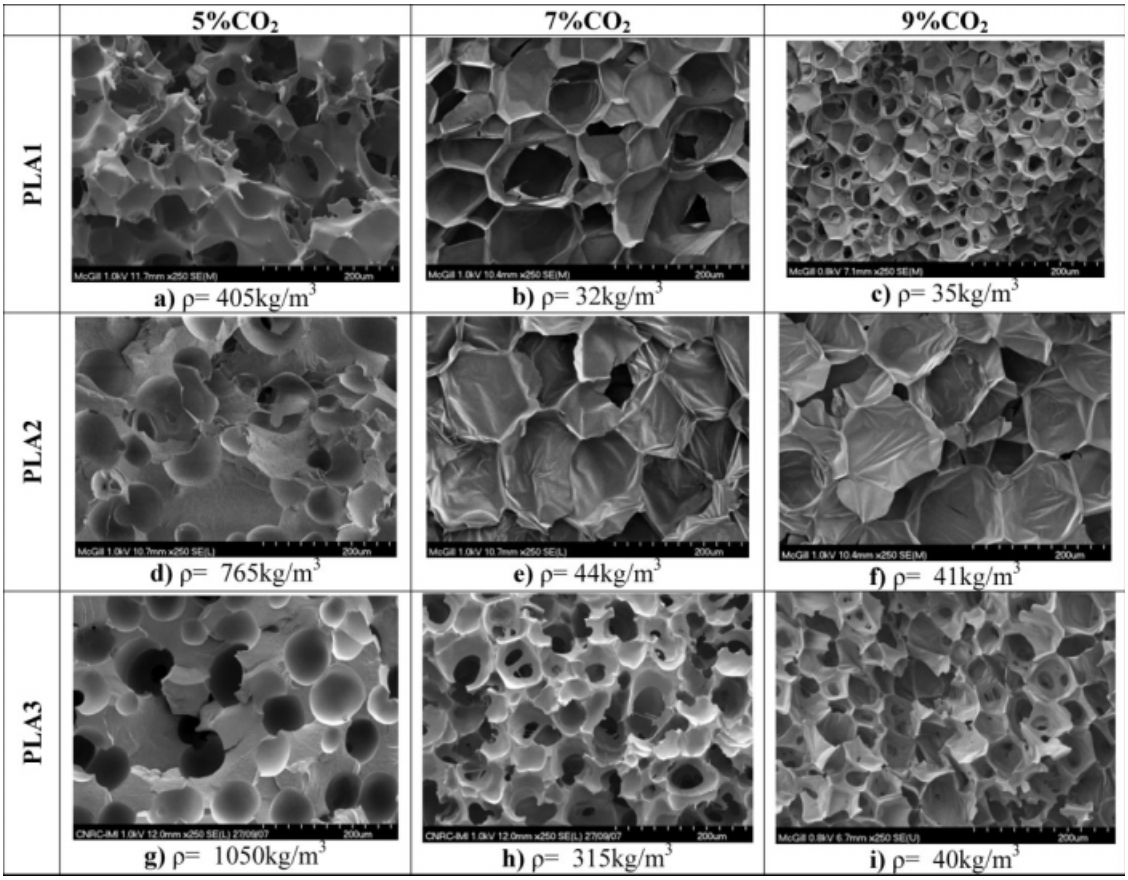

Figure 4 SEM micrographs of fractured foams obtained from the three grades of PLA with 5, 7, and 9% CO_2 using the 2-mm die.

was possible to achieve low-density foams at lower CO_2 content than with the amorphous PLA3. More importantly, low-density foams were achieved only in conditions that led to significant crystallinity development (i.e., 7 and 9% CO_2). The amorphous PLA3 could still be foamed but required higher CO_2 concentration.

The thermal analysis and foam morphology presented above were for foams produced with a 2-mm capillary die. A similar analysis was carried out on PLA foams produced with 1.5 and 3.5-mm dies to examine the effect of the die diameter. Table I presents the foam densities and crystallinity obtained by DSC and further confirmed by XRD analysis for all the foams. It was expected that a smaller diameter die would induce a higher pressure gradient and higher shear rates in the die, possibly resulting in better foam nucleation and shear-induced

TABLE I
Crystallinity (X_C) from DSC, Crystalline Peak Intensity Ratio from XRD and the Corresponded Densities for PLA Foamed at 10 kg/h with Different Dies

		Crystallinity (%)/Peak intensity ratio (%)/Foam density (kg/m^3)								
	Die diameter (mm)	5% CO_2			7% CO_2			9% CO_2		
		X_C	$I_C/(I_C + I_A)$	ρ	X_C	$I_C/(I_C + I_A)$	ρ	X_C	$I_C/(I_C + I_A)$	ρ
PLA1	1.5	9	0	690	11	32	45	22	37	35
	2.0	6	19	405	25	40	32	45	52	35
	3.5	6	20	820	12	30	280	14	35	35
PLA2	1.5	0	0	680	9	17	43	15	32	48
	2.0	0	0	765	7	18	45	19	24	41
	3.5	0	0	944	0	17	166	11	19	35
PLA3	1.5	0	0	680	0	0	460	0	0	250
	2.0	0	0	1050	0	0	315	0	0	40
	3.5	0	0	585	0	0	850	0	0	570

crystalline nucleation. The low-density PLA1 foams had a crystallinity content between 25 and 45% while low-density PLA2 ones had between 7 and 20% and were obtained with 2-mm die. For the amorphous PLA3, low-density foams were achieved only with the 2-mm die using 9% CO_2. Therefore, unexpectedly, the 2-mm die presented more favorable conditions for foaming even in the absence of crystallization. Perhaps, the nucleation density, exit velocity, and cooling rate obtained with the 2-mm die provide a narrow operating window in which better foams can be produced. Obviously, however, crystallinity development during foaming extended the foaming window to lower blowing agent concentrations and to a wider range of operating conditions than in the case of the amorphous material.

Figure 5 presents SEM micrographs of PLA1 foams obtained with 7% CO_2 while varying the die diameter. The foam obtained using 1.5-mm die had the smallest cells, around 50 μm and a uniform cell dimension distribution. For the 2-mm die, the cell dimension was roughly increased to around 75 μm and remained uniformly distributed. The foam obtained with this die had the lowest density and the highest crystalline level. For the 3.5-mm die, a bimodal foam morphology with large cells, around 500 μm, and small cells, around 50–100 μm, was observed. The lack of morphological uniformity in this case of 3.5-mm die was probably due to premature phase separation caused by the lower pressure drop. The phase-separated CO_2 fraction formed pockets of gas that led to the formation of large cells.

In Figure 6, the effect of extrusion flow rate is investigated. When the flow rate was 5 kg/m^3, a bimodal foam structure was once again obtained. In this case, it is the lower flow rate that lowered the pressure gradient and led to premature phase separation. The cell size distribution was narrowed and the average cell size decreased as the flow rate was increased to 7.5 kg/m^3 and then to 10 kg/m^3. All these foams had low densities, around 30–40 kg/m^3, but the crystallinity increased with the flow rate from 11 to 45%.

The ability of materials to crystallize can be quantified by the examination of the crystallization rate as a function of temperature. One way to do this is to report the crystallization half-time. The half-time is defined as the time needed to develop 50% of the maximum crystallinity in a sample that was initially completely amorphous. In our study, the crystallization half-time of PLA was theoretically assessed using the basic isothermal crystallization kinetics of polymers and taking into account the effect of dissolved CO_2. The degree of crystallinity X_C at time t for a heterogeneous nucleation is given by the Avrami equation[31–33]:

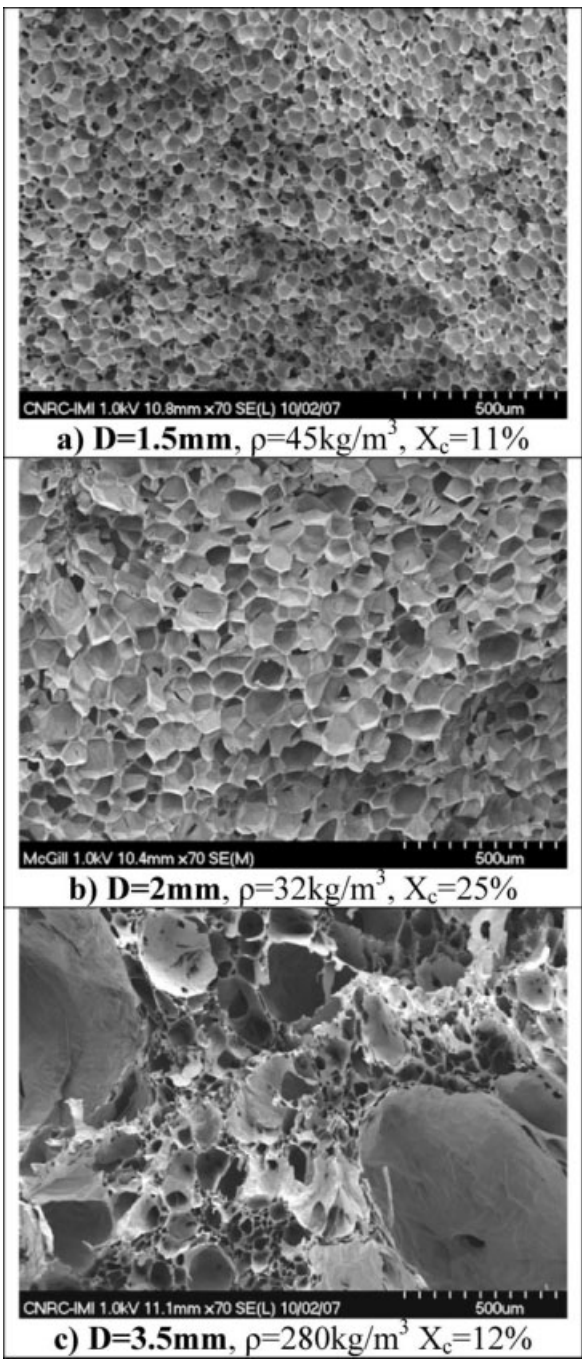

Figure 5 Effect of die diameter on the morphology of PLA1 foams produced at 10 kg/m^3 using 7% CO_2.

$$-\ln\left(1-\frac{X_C(t)}{X_\infty}\right)=\frac{1}{X_\infty}\frac{\rho_C}{\rho_l}K_f\dot{G}^3\bar{N}t^n \qquad (1)$$

where X_∞ is the crystallinity at the completion of the crystallization, ρ_C, ρ_l are the densities of crystalline and amorphous phases, $K_f = 4\pi/3$ is a shape factor, $\dot{G}$ is the crystal linear growth rate, $\bar{N}$ is the number of nuclei, and n is the Avrami exponent. The only temperature-dependent parameters in eq. (1) are $\dot{G}$ and $\bar{N}$ and this temperature dependency

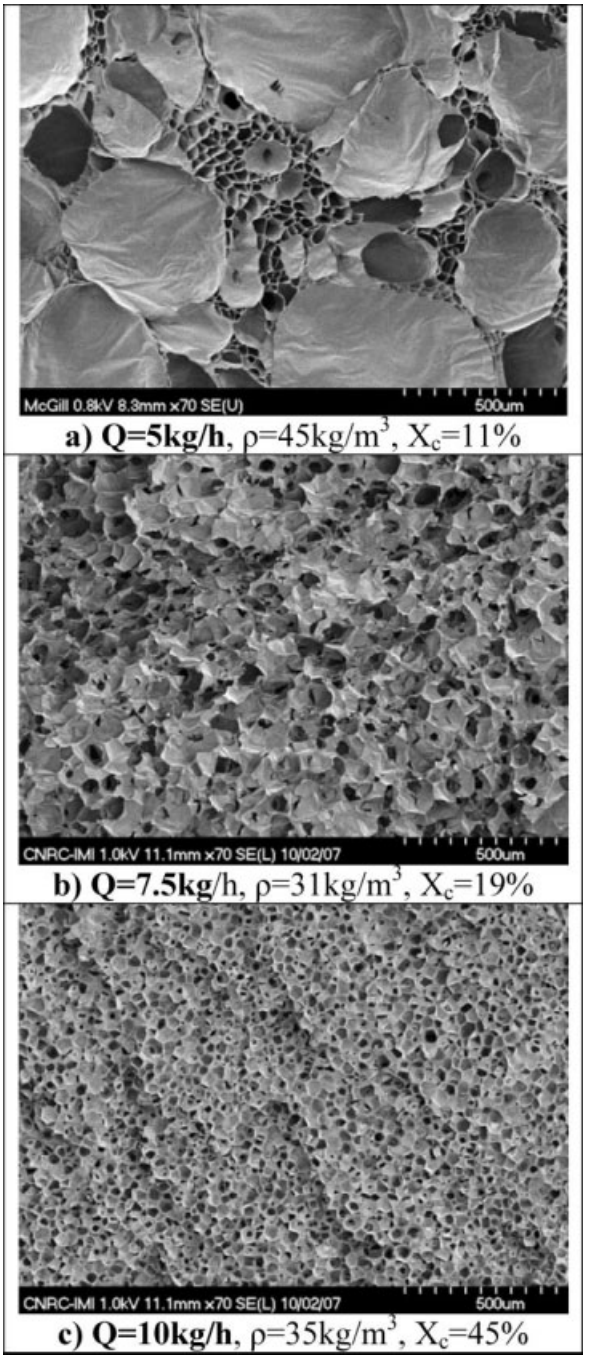

Figure 6 Effect of flow rate on the morphology of PLA1 foams produced with the 2-mm die using 9% CO_2.

has been described by the Takayanagi–Kusumoto equations[33,34]:

$$\log \dot{G} = \log \dot{G}_0 - \frac{\rho C_1 T_C}{\left(T_C - \left(T_g - 51,6\right)\right)^2} - \frac{C_2 T_m}{T(T_C - T_m)} \tag{2}$$

$$\log \bar{N} = \log \bar{N}_0 - \frac{C_3 T_m}{T_C(T_C - T_m)} \tag{3}$$

In eqs. (2) and (3), $\dot{G}_0$, $\bar{N}_0$, C_2, and C_3 are material characteristic parameters independent of temperature, C_1 is a universal constant, and T_g, T_c, and T_m are the glass transition, crystallization, and melting temperature, respectively. Isothermal crystallization data obtained with PLA1 were used to determine ρ, C_2, and C_3 specific to PLA. The presence of dissolved gas and pressure on the T_g and T_m of the polymer has been taken into account as independent parameters using eqs. (4) and (5)[25,33]:

$$T_g = T_g^0 + \alpha_g^P \times P - \alpha_g^{CO_2} \times P_{CO_2} \tag{4}$$

$$T_m = T_m^0 + \alpha_m^P \times P - \alpha_m^{CO_2} \times P_{CO_2} \tag{5}$$

where T_g^0 and T_m^0 are the temperature values measured for the pure polymer at atmospheric pressure, α_g^P and α_m^P are the pressure shift factors for T_g and T_m, P is the static pressure value, $\alpha_g^{CO_2}$ and α_m^{CO2} are the CO_2 shift factors for T_g and T_m, and P_{CO_2} is the pressure level of CO_2. At equilibrium conditions, the dissolution of a compressed gas in a melted polymer follows Henry law and the molar fraction of the dissolved gas, [gas], is proportional with the pressure P. The pressure level can be expressed by Henry's law as follows[35]:

$$P = \frac{[\text{gas}]}{K_H} \tag{6}$$

By combining eqs. (1)–(6) and using the parameters summarized in Table II, we have calculated the theoretical effect of pressurized CO_2 on the crystallization of PLA1.

Figure 7 presents the crystallization half-time calculated as a function of temperature for different CO_2 concentrations at the equilibrium CO_2 pressure. The enclosed graph represents the typical experimental isothermal crystallization curves for the PLA1 and PLA2 at 100°C. At that temperature, PLA1 takes over 40 min to reach half of its maximum crystallinity, whereas PLA2 has completed less than 30% of its crystallinity after 6 h of annealing. The different theoretical curves presented in Figure

TABLE II
Parameters Used for Crystallinity Calculations in Presence of CO_2 Plasticization

Parameter	Value	References
X_∞	0.4	30
ρ_C	1290 kg/m^3	25
ρ_l	1248 kg/m^3	25
$\dot{G}_0$	1.5 μm/min	36
$\bar{N}_0$	1e^{-8} μm^{-3}	13
C_1	900	33
α_g^P	0.173 K/MPa	37
α_m^P	0.173 K/MPa	37
$\alpha_g^{CO_2}$	3.66 K/MPa	25
$\alpha_m^{CO_2}$	2.18 K/MPa	25
K_H (448 K)	0.0154 MPa^{-1}	35
CO_2 solubility (448 K)	0.94% CO_2 MPa^{-1}	35

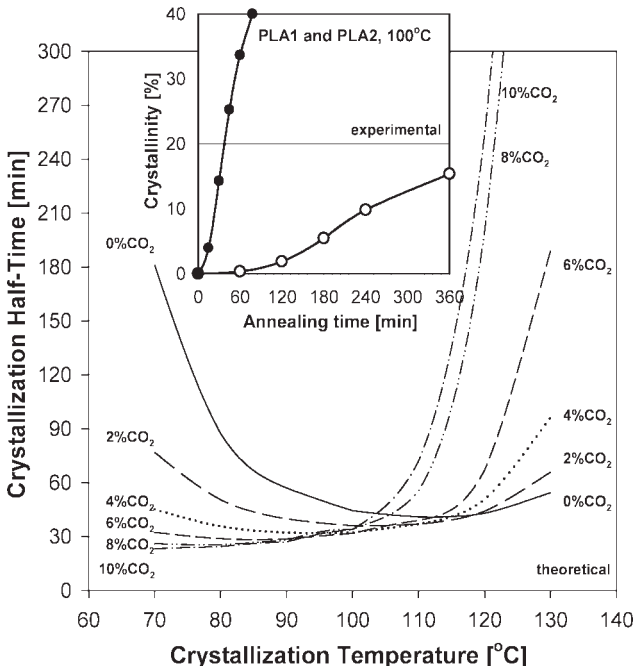

Figure 7 Crystallization half-time as a function of temperature at different CO_2 concentrations obtained from eqs. (1)–(6). Included graph represents the experimental isothermal crystallization curves for PLA1 and PLA2.

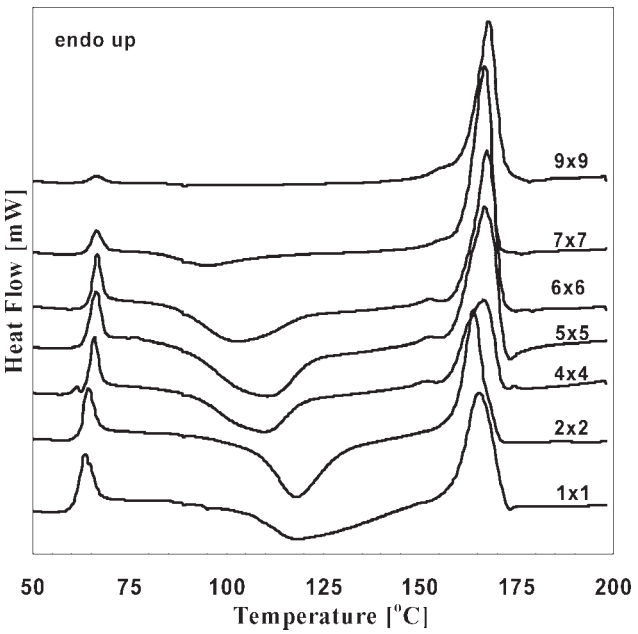

Figure 8 DSC traces for PLA1 after different stretching ratios at 100°C.

7 are for increasing CO_2 concentration. In the absence of CO_2, PLA showed a minimum crystallization half-time of 41 min for an optimum crystallization temperature of 110°C. The minimum half-time decreased with CO_2 concentration to reach 23 min at 10% CO_2. At this concentration, the optimal crystallization temperature was also decreased down to 70°C. Obviously, the plasticization effect provided by CO_2 and described by eqs. (1)–(6) is not sufficient to explain the rapid crystallinity development observed in the few seconds required to expand and cool the PLA foams. Even if a level of 20% CO_2 was used in our calculation, the CO_2 plasticization effect decreases the half-time only to around 16 min and the optimal crystallization temperature down to 20–30°C. Thus, other factors such as biaxial stretching and CO_2 induced nucleation must be considered to explain the rapid crystallinity growth in extrusion foaming.

With the purpose of separating these effects, two different experiments were done. First, the effect of biaxial stretching on crystallinity development was determined for PLA1 and PLA2 cast sheets subjected to different biaxial deformations at 100°C. Second, the effect of CO_2 concentration on the level of crystallization was examined by subjecting PLA1 and PLA2 cast sheets to CO_2 pressure for different times. Figure 8 shows the DSC traces for PLA1 after biaxial deformation up to 9 × 9. The speed of the deformation used for these tests, 1 m/min, was a coarse approximation of the maximum expansion speed of foam cell walls during foaming. For the unstretched PLA1 sheet (1 × 1), the crystallization exotherm was broad and centered around 118°C. As the stretch ratio was increased, the crystallization exotherm was narrowed, shifted to lower temperatures and finally completely disappeared at a stretch ratio of 9 × 9. At this point, the sheet was completely crystallized

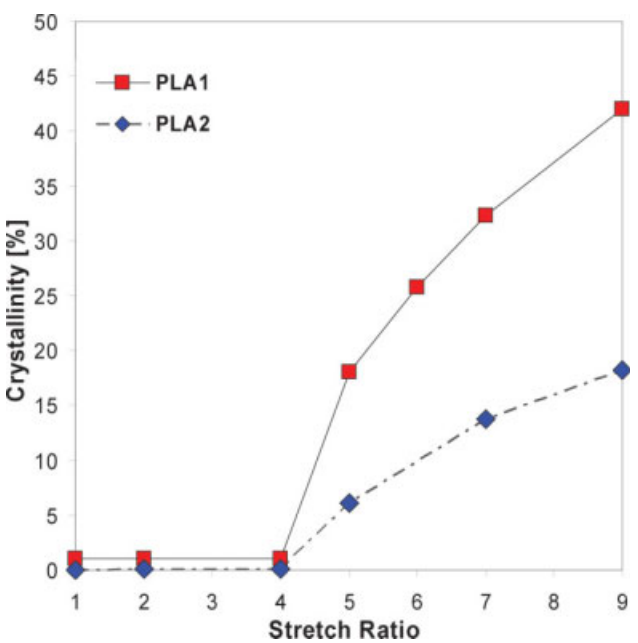

Figure 9 Crystallinity developed in PLA sheets after biaxial stretching at 100°C as a function of stretch ratio. [Color figure can be viewed in the online issue, which is available at www.interscience.wiley.com.]

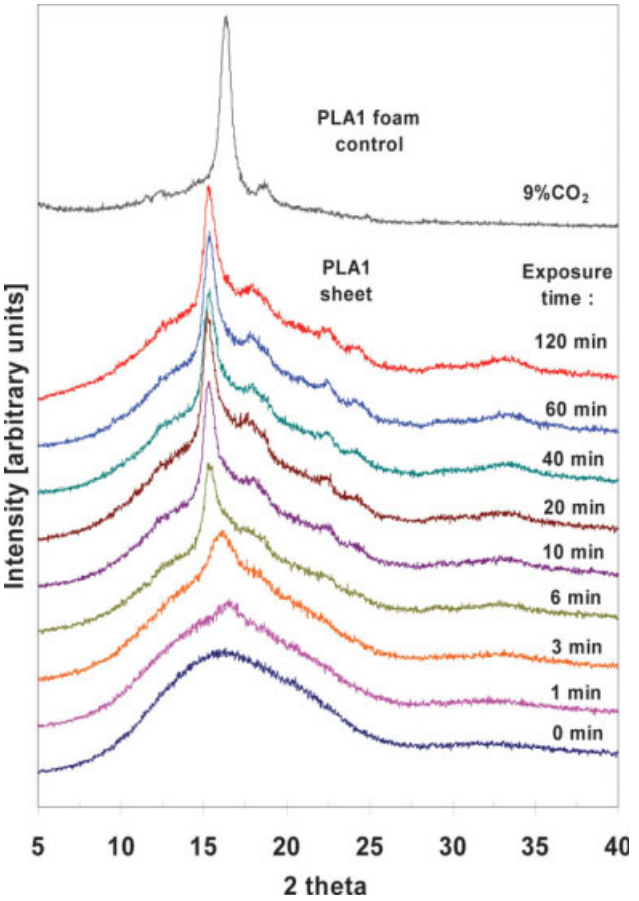

Figure 10 X-ray scattering intensity for PLA1 sheets exposed to 6 MPa of CO_2 for selected durations. [Color figure can be viewed in the online issue, which is available at www.interscience.wiley.com.]

during the biaxial stretching. A similar behavior was observed for PLA2 sheets.

Figure 9 compares the crystallinities attained in PLA1 and PLA2 sheets as a function of biaxial stretch ratio. The two PLA sheets, initially amorphous, did not develop any crystallinity up to a deformation of 4 × 4. For deformations higher than 4 × 4, PLA1 crystallized more rapidly and to a higher extent than PLA2. At a deformation of 9 × 9, PLA1 and PLA2 crystallinity was 42 and 18%, respectively . These values are close to measured values for foamed materials with 9% CO_2 (i.e., 45 and 19%, respectively). It should be noted that the stretching was carried out in a relatively short period of time. For example, the 4 × 4 stretching ratio was achieved in 15 s. Therefore, contrary to the theoretical plasticization effects discussed earlier, the biaxial stretching can induce significant crystallinity in a time frame that is similar to that expected for the foam expansion and cooling. Therefore, a biaxial deformation could be sufficient to induce an appreciable crystallization degree even without CO_2 to plasticize PLA.

To investigate the isolated effect of CO_2, unstretched PLA sheets were subjected to a CO_2 pressure of 6 MPa for different exposure times at room temperature. To avoid crystallization on heating and CO_2 plasticization effects during crystallinity measurements, XRD was preferred over DSC to determine the sample's crystallinity. Figure 10 shows XRD scans for PLA1 sheets that were subjected to high CO_2 pressure for time of 1 min up to 2 h. The unexposed sample (0 min) displayed no crystalline peaks and can be used as an amorphous reference. The scan for PLA1 extruded foam with the crystalline content of 45% can also be used as a reference of a fully crystallized sample. The scans typically exhibited an amorphous hump, a sharp crystallinity peak at around $2\theta = 16.5°$ and a little one around $2\theta = 18.9°$ typical of PLA crystals. The characteristic crystalline peak progressively increased in intensity with the time of exposure. Even after 1 min of CO_2 exposure, a small crystalline peak appeared at $2\theta = 16.7°$. The peak intensity increased as the exposure time was increased up to 20 min and was also shifted down to $2\theta = 15°$ indicating reorganization in the crystalline structure. Secondary peaks at around $2\theta = 18.9°$, 22.7°, and 24.5° characteristic of PLA crystals and also visible in the crystalline foam reference became present at the exposure times of 6 min and increased in size on further exposure. For exposure times greater than 20 min, the XRD scans

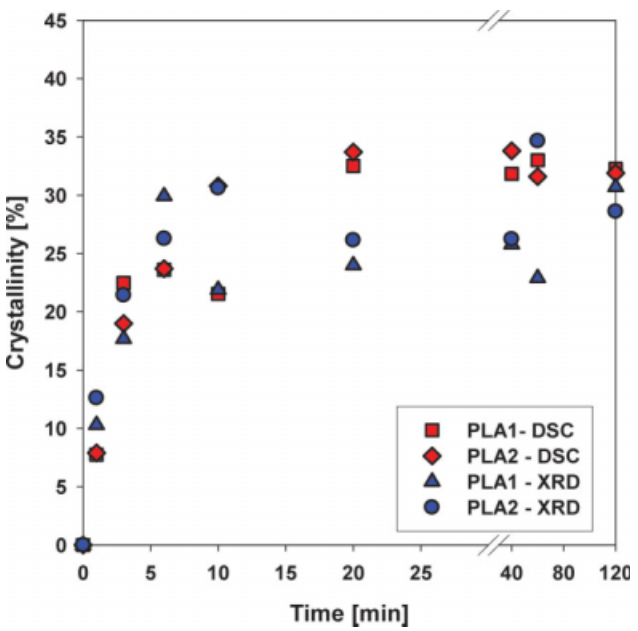

Figure 11 Calculated crystallinity from DSC and XRD runs for PLA1 and PLA2 sheets as a function of exposure time at 6 MPa of CO_2. [Color figure can be viewed in the online issue, which is available at www.interscience.wiley.com.]

did not change significantly, indicating that the CO_2-induced crystallization had reached a plateau value. Similar XRD scans were carried out on PLA2 sheets and the crystalline peak ratios were calculated.

Figure 11 compares the DSC and XRD crystallinity data for PLA1 and PLA2 sheets as a function of CO_2 exposure time. The two PLA grades exhibited similar trends with a maximum crystallinity around 30% attained after 20 min of CO_2 exposure. Therefore, CO_2 can also induce significant PLA crystallization even at room temperature. In the current experiments, PLA crystallization in the presence of CO_2 did not proceed to levels as high as for biaxial stretched samples. Crystallization also occurred more slowly than in the stretching experiments. It should be noted however that the CO_2 soaking experiments were carried out at the room temperature, hence well below the optimum crystallization temperature. Thus, the significant crystallization observed in these unfavorable conditions supports the hypothesis that CO_2 accelerates PLA crystallization. The fact that this effect was not captured through the calculations based on plasticization and T_g depression presented earlier indicates that in addition to changing the PLA chain mobility, CO_2 has a nucleating ability that is not accounted for in the models described by eqs. (1)–(6). It can then be expected that the effect of strain and CO_2 will be combined in the PLA foaming process leading to the high crystallinity levels as discussed above.

In a previous study using PLA2, peculiar cell rupture features such as highly cavitated cell walls were found using scanning electron microscopy at high magnification.[29] It was then assumed that the cavities developed in the amorphous regions. It was therefore interesting in this work to confirm if this feature could be systematically reproduced with the higher crystallinity PLA1 or suppressed using amorphous PLA3. Figure 12 presents micrographs of single cell walls in PLA1 to PLA3 foams obtained with 5, 7, and 9% CO_2. A highly cavitated structure that we will refer to as a "lace structure" was found in the semicrystalline PLA1 and PLA2. This lace structure was observed in cell walls that were ruptured as well as in unruptured ones. It disclosed a network of very small cavities separated by fibrils. In some area, larger cavities with nonuniform dimensions have appeared due to the rupture of consecutive fibrils. Hence, the micrographs were duplicated using higher magnifications to better describe the variety of cell wall textures and rupture types. At 5% CO_2, PLA was scarcely foamed and only PLA1 exhibited the lace structure. At this low blowing agent concentration, small changes in foaming conditions modified the cell rupture resulting in fractured cell walls without lace (case A-A*), with macroscopic cracks passing through the lace structure (case B-B*) or could present loose networks of thick and fine fibrils (case C-C*). At the same CO_2 concentration, PLA2 and PLA3 showed only a coarse cell structure and no cavitation features. At the higher CO_2 concentrations, which lead to highly expanded foams, the semicrystalline PLA1 and PLA2 both presented the lace archetype. The lace structures formed at 7 and 9% CO_2 differed only in the dimension of cavities and fibrils. At 7% CO_2, cavities around 150 nm in diameter were slightly elongated in the same direction as the thicker fibrils. Thinner and shorter fibrils, approximatively 10 nm in width, separated the cavities. At 9% CO_2, finer cavities, around 75 nm, and finer fibers were found. In the case of PLA3, no lace structures were present; only macrovoids between 2 and 10 μm in diameter were found in foam cell walls at 7 and 9% CO_2. These voids are two orders of magnitude greater than the cavities observed in the semicrystalline lace structures. This supports the assumptions that the lace structure is intimately related to the presence of crystalline domains in the PLA cell walls upon cell growth.

DISCUSSION

It is interesting to reflect on the mechanisms that guide cell wall cavitation and to the role of crystallization in foaming. Since the cavitated walls were present only in highly expanded foams, it is a strong indication that the cavitation occurred during the cell growth stage. The ordered state in which the cavities were found leads one to hypothesize that they have formed in the amorphous zones between growing crystallites and thus that formation of a minimal quantity of crystallites occurred before expansion. Since the material was able to flow in the extrusion die, it is obvious that only a small amount of crystal nuclei was present in the flowing material, more or less floating in the amorphous mass. During cell expansion, the biaxial stresses were relieved by the formation of cavities that have appeared in the amorphous "weak point" between crystallites. As long as these cavities did not release all CO_2, the driving force of the wall stretch was maintained, the expansion continued, and it developed more crystallinity. The fibrils that separate the cavities were stretched and the cavities size and number increased to a point where some walls ruptured through the formation of a macrocrack that propagated through the weakened lace structure. It can be safely assumed that the significant level of crystallinity found in the final state of the foams were formed during the expansion phase and possibly helped stabilize the foam structure thus expanding the foamability window. By contrast with the semicrystalline PLA, only large macrovoids were developed in the

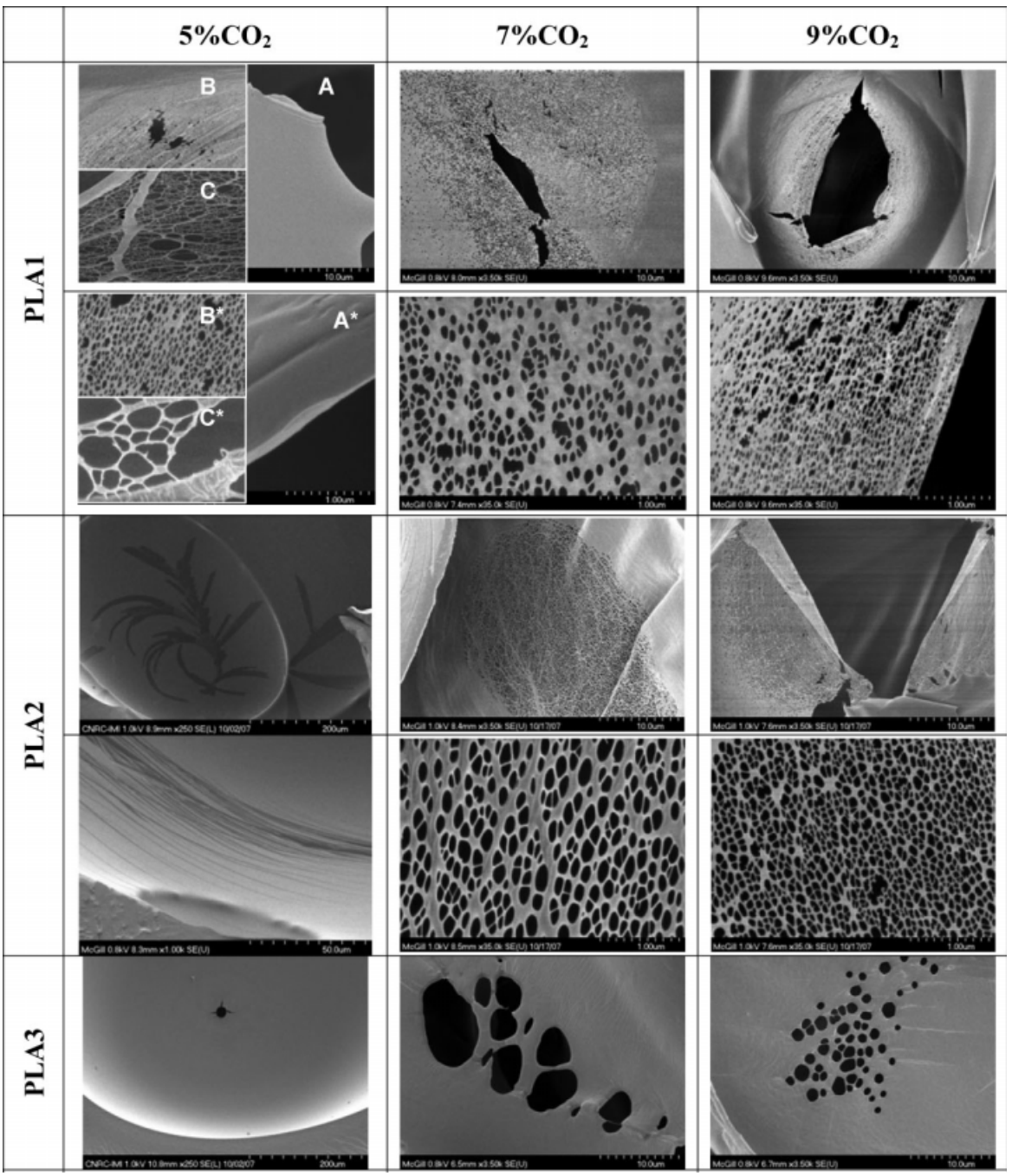

Figure 12 High magnification scanning electron micrographs of single cell walls in PLA1, PLA2, and PLA3 foams.

amorphous PLA3. The ability to cavitate may present some advantages in terms of fracture energy dissipation and thus could improve the ability of a brittle material such as PLA to sustain the high deformation during foaming. More importantly, however, these observations show that PLA crystallites were already present in the expanding foam. This is far from being trivial or expected and shows that in a slowly crystallizing material, the process conditions can be selected such that crystal nuclei can be formed at the same time or even before foam nucleation. As we will now discuss, the crystallites may even contribute to nucleate foaming.

Two important general observations regarding PLA foaming were made in this study. First, it was observed that the blowing agent concentration necessary to attain high foam expansion was decreased whenever PLA was able to crystallize. Second, the transition between poorly expanded foams and highly expanded ones was extremely quick. These two observations are not typical in polymer foaming. The fact that the quality of foams was improved in

the PLA3 < PLA2 < PLA1 order infers that the crystalline development played an important role in the foaming process. As explained above, it seems likely that crystallites appeared before the start of the foaming process and then crystal nuclei were already present in the pressurized PLA/CO_2 solution even prior die exit. A potential explanation for the fact that the same critical CO_2 level was necessary to obtain significant crystallization as well as in achieving highly expanded foams could be that crystalline nuclei are also acting as a foam nucleation site. It has been shown in batch-foaming experiments that PLA crystal nuclei can act as foam nucleation sites.[38] Similar results were seen in PET.[39] In the extrusion sequence of operation, crystalline nucleation could be induced by CO_2 and in turn, this could dramatically increase the foam nucleation density. Since PLA crystal growth is relatively slow, it is conceivable that crystal nuclei can coexist as a minor phase in a flowing amorphous PLA matrix. This is supported by the more gradual density decrease observed with the amorphous PLA. In this case, however, one could wonder why it is even possible to produce low-density foams. The answer may relate to a second mechanism involving an increase in foam nucleation density. It is noteworthy that the critical pressure of CO_2 is around 7.2 MPa. According to previously published CO_2 solubility data in PLA, the equilibrium CO_2 concentration corresponding to a vapor pressure of 7.2 MPa is around 7% CO_2.[29] Thus, the use of CO_2 concentration in excess of 7% implies that the CO_2 will be in a supercritical state. This could lead to CO_2 clusters formation that could also provide foam heterogeneous nucleation that progressively could improve the foam quality at increasing blowing agent concentration. In the semicrystalline PLA grades, both the crystal formation and the CO_2 clusters should contribute to increase the foam nucleation density leading to the observed wider operation window.

CONCLUSIONS

The interactions between process conditions, composition, crystallization, and foam properties were investigated for PLA extrusion-foamed using CO_2 as a physical blowing agent. The crystalline content of PLA foams was increased with CO_2 concentration and its *L*-LA content. At low CO_2 concentrations, PLA was scarcely foamed and presented low crystallinity. Above a critical CO_2 level, foams with low densities, around 35 kg/m^3, could be produced. This critical level was decreased when more readily crystallizable PLA grades were used. Independent experiments showed that pressurized CO_2 and biaxial stretching can both significantly increase the PLA crystallization rate. A peculiar cavitation phenomena observed in the cell wall of highly crystalline foams led to the conclusion that PLA crystallites are present during the foam nucleation state. The assumed sequence of events in the foaming of semicrystalline PLA was that PLA crystal nuclei formation was induced by CO_2 in the extrusion die before the foaming step. These crystalline nuclei significantly increased the foam nucleation density. Crystallinity was further developed by the biaxial stretching occurring during the foam expansion leading to highly expanded foams and to cavitated cell walls. Supercritical CO_2 clusters were also shown to potentially increase the foam nucleation density and to be an important factor in the fabrication of amorphous PLA foams.

The authors thank François Vachon, Chantal Coulombe, and Michel Carmel for their technical support.

References

1. Garlotta, D. J Polym Environ 2001, 9, 63.
2. Bigg, D. M. Adv Polym Technol 2005, 24, 69.
3. Kale, G.; Kijchavengkul, T.; Auras, R.; Rubino, M.; Selke, S. E.; Singh, S. H. Macromol Biosci 2007, 7, 255.
4. Dorgan, J. R.; Lehermeier, H. J.; Palade, L. I. Cicero J Macromol Symp 2001, 175, 55.
5. Auras, R.; Singh, S. P.; Singh, J. J Test Eval 2006, 34, 1.
6. Urbanovici, E.; Schneider, H. A.; Brizzolara, D.; Cantow, H. J. J Therm Anal 1996, 47, 931.
7. Yasuniwa, M.; Tsubakihara, S.; Iura, K.; Ono, Y.; Dan, Y.; Takahashi, K. Polymer 2006, 47, 7554.
8. Yasuniwa, M.; Tsubakihara, S.; Sugimoto, Y.; Nakafuku, C. J Polym Sci Part B Polym Phys 2004, 42, 25.
9. Di Lorenzo, M. L. Macromol Symp 2006, 234, 176.
10. Di Lorenzo, M. L. J Appl Polym Sci 2006, 100, 3145.
11. Yasuniwa, M.; Iura, K.; Dan, Y. Polymer 2007, 48, 5398.
12. Tsuji, H.; Takai, H.; Saha, S. K. Polymer 2006, 47, 3826.
13. Nam, J. Y.; Ray, S. S.; Okamoto, M. Macromolecules 2003, 36, 7126.
14. Ray, S. S.; Maiti, P.; Okamoto, M.; Yamada, K.; Ueda, K. Macromolecules 2002, 35, 3104.
15. Day, A.; Nawaby, A. V.; Liao, X. J Therm Anal Calorim 2006, 86, 623.
16. Zhang, J.; Jiang, L.; Zhu, L. Biomacromolecules 2006, 7, 1551.
17. Mathew, A. P.; Oksman, K.; Sain, M. J Appl Polym Sci 2006, 101, 300.
18. Labrecque, L. V.; Kumar, R. A.; Davé, V.; Gross, R. A.; McCarthy, S. P. J Appl Polym Sci 1997, 66, 1507.
19. Kulinski, Z.; Piorkowska, E. Polymer 2005, 46, 10290.
20. Jacobsen, S.; Fritz, H. G. Polym Eng Sci 1999, 39, 1303.
21. Baiardo, M.; Frisoni, G.; Scandola, M.; Rimelen, M.; Lips, D.; Ruffieux, K.; Wintermantel, E. J Appl Polym Sci 2003, 90, 1731.
22. Ljungberg, N.; Wesslen, B. Biomacromolecules 2005, 6, 1789.
23. Piorkowska, E.; Kulinski, Z.; Galeski, A.; Masireka, R. Polymer 2006, 47, 7178.
24. Li, H.; Huneault, M. A. Polymer 2007, 48, 6855.
25. Takada, M.; Hasegawa, S.; Ohshima, M. Polym Eng Sci 2004, 44, 186.
26. Kokturk, G.; Serhatkulu, T. F.; Cakmak, M.; Piskin, E. Polym Eng Sci 2002, 42, 1619.
27. Chapleau, N.; Huneault, M. A.; Li, H. Int Polym Process 2007, 22, 402.

28. Reignier, J.; Gendron, R.; Champagne, M. F. Cell Polym 2007, 26, 83.
29. Mihai, M.; Huneault, M. A.; Favis, B. D.; Li, H. Macromol Biosci 2007, 7, 907.
30. Fischer, E. W.; Sterzel, H. J.; Wegner, G. Kolloid-Z u Z Polym 1973, 251, 980.
31. Avrami, M. J Chem Phys 1939, 7, 1103.
32. Avrami, M. J Chem Phys 1940, 8, 212.
33. Ito, H.; Tsutsumi, Y.; Minagawa, K.; Takimoto, J.; Koyama, K. Colloid Polym Sci 1995, 273, 811.
34. Takayanagi, M.; Kusumoto, N. Kogyo Kagaku Zasshi 1959, 62, 587.
35. Lian, Z.; Epstein, S. A.; Blenk, C. W.; Shine, A. J Supercrit Fluids 2006, 36, 107.
36. Tsuji, H.; Tezuka, Y.; Saha, S. K.; Suzuki, M.; Itsuno, S. Polymer 2005, 46, 4917.
37. Nakafuku, C. Polym J 1993, 26, 680.
38. Liao, X.; Nawaby, A. V.; Day, M. P. M. S. E. Preprints 2006, 95, 613.
39. Baldwin, D. F.; Shimbo, M.; Suh, N. P. Trans ASME 1995, 117, 62.